IEEE Access
Multidisciplinary ⋮ Rapid Review ⋮ Open Access Journal

Received 21 January 2024, accepted 11 February 2024, date of publication 21 February 2024, date of current version 8 March 2024.

Digital Object Identifier 10.1109/ACCESS.2024.3368755

RESEARCH ARTICLE

Data-Augmentation Based CBAM-ResNet-GCN Method for Unbalance Fault Diagnosis of Rotating Machinery

HAITAO WANG[1], XIYANG DAI[1], LICHEN SHI[1], MINGJUN LI[1], ZELIN LIU[1], RUIHUA WANG[1], AND XIAOHUA XIA[2]

[1]School of Mechanical and Electrical Engineering, Xi'an University of Architecture and Technology, Xi'an 710055, China
[2]Key Laboratory of Road Construction Technology and Equipment of Ministry of Education, Chang'an University, Xi'an 710064, China

Corresponding author: Xiaohua Xia (xhxia@chd.edu.cn)

This work was supported the Fundamental Research Funds for the Central Universities, Chang'an University (CHD); and the Key Laboratory of Road Construction Technology and Equipment (Chang'an University), Ministry of Education of the People's Republic of China (MOE), under Grant 300102250503.

ABSTRACT In practical engineering scenarios, machines are seldom in a faulty operating state, so it is difficult to get enough available sample data to train the fault diagnosis model, leading to the problem of the small and unbalanced number of rotating machinery fault samples and low fault diagnosis accuracy. To solve this problem, this paper introduces a novel approach to machinery fault diagnosis. This approach involves the integration of a Convolutional Attention Residual Network (CBAM-ResNet) with a Graph Convolutional Neural Network (GCN). Firstly, to comprehensively exploit time-domain information from one-dimensional vibration signals, this study utilize Gram Angular Field (GAF) coding to transform traits of vibration signals into two-dimensional image characteristics. The resultant two-dimensional image is then expanded by applying the Wasserstein Distance Gradient Penalty Generation Adversarial Network (WGAN-GP) to produce a representative sample image. Secondly, the image is input to CBAM-ResNet to perform focused feature extraction and construct the feature matrix. Lastly, the adjacency matrix is derived through Graph Generation Layer (GGL); subsequently, the feature matrix and adjacency matrix are utilized as inputs for the GCN. After deep feature extraction, fault feature classification is executed via Softmax. Performance tests were conducted using the Case Western Reserve University bearing dataset and the planetary gearbox dataset. The method demonstrated remarkable results, achieving an accuracy of over 99% on the unbalanced dataset and surpassing 98% in 0dB noise compared to various other models. This illustrates the effectiveness and feasibility of the proposed method.

INDEX TERMS Attentional mechanism, fault diagnosis, gram angle difference field, generative adversarial network, graph neural network (GCN), rotating machinery.

I. INTRODUCTION

In the context of rapid modern industrial development, mechanical equipment is progressively advancing towards precision, high grade, and automation, and the information it contains is also moving towards big data and big storage lean-in [1]. Bearings and gears, integral and indispensable mechanical equipment components, are pivotal in ensuring operational health and production safety. Such failures could endanger the operational normalcy of rotating mechanical equipment, posing risks to human safety and project advancement [2], [3]. Consequently, monitoring conditions and diagnosing faults pertaining to bearings and gears stand as pivotal subjects of inquiry for national and international experts [4]. An especially crucial facet of fault diagnosis resides in feature extraction, with the efficacy and precision of the model being directly contingent on the caliber of feature extraction. For early machine failures, several issues emerge: initially, during the incipient stages of bearing or gear failure, the failure characteristics are weak,

The associate editor coordinating the review of this manuscript and approving it for publication was Mehrdad Saif.

thereby affecting efficacious feature extraction; secondly, the operation of machinery invariably entails concurrent noise presence, thus heightening the intricacy associated with feature extraction processes. In addressing the challenges above, Li et al. [5] proposed a multi-layer reconfiguration filter tailored to detect subtle faults in rolling bearings early. This innovative method synergistically integrates the strengths of wavelet transform and variational decomposition to mitigate noise interference upon faint signals. Similarly, Liu and Ren [6] introduced the Maximum Correlation Cliff Deconvolution (MCKD) technique, especially in the case of impulsive vibration signals containing periodicity, which is effective in suppressing harmonics and noise components in gearboxes to accurately identify gear faults. Biao et al. [7] introduced a rapid sparsity-enabled feature energy ratio method. In the first stage, they automatically segmented the spectrum to identify fault feature bands. The second stage further refined this by applying an enhanced sparse coded shrinkage denoising (SCSD) method, effectively capturing early fault features in rotating motors. While the aforesaid proposed approaches effectively address the challenges above, Fault diagnosis in the context of big data requires enough available data to train models. However, the current landscape is marred by a dearth of available fault samples and an imbalanced dataset, training deep learning models becomes challenging, and addressing the issue of imbalanced sample data while concurrently ensuring efficacious feature extraction emerges as an imperative in augmenting the model's accuracy.

To address this problem, Goodfellow et al. [8] introduced the Generative Adversarial Net (GAN) concept, offering a potent approach to address the scarcity of minority class samples. Originally conceived as a framework for image generation, GAN encountered challenges related to subpar image quality primarily due to training instability. Consequently, many research endeavors emerged, focusing on diverse variants of adversarial networks in a concerted effort to enhance the generated image quality. Aiming at the problem of difficulty in obtaining enough samples resulting in low accuracy, Yang et al. [9] proposed the use of Conditional Generation Networks (CGANs) to generate new samples, which are then pre-processed and fed into 2-D-CNN for feature extraction and classification of bearing faults. Farajzadeh-Zanjani et al. [10] propose a new generative adversarial network for the problem that faulty samples are much less than normal samples and thus lead to inaccurate classification. This novel Adversarial Classroom Imbalance Learning (ACIL) employs a novel loss function for training. In addition, an inclusive data-driven scheme for classifying network attacks and faults is designed to effectively improve fault sample classification. Li et al. [11] proposed WGAN combined with long and short-term memory full convolutional network (LSTM-FCN) to solve the problem of difficult sample collection, which leads to low accuracy. The generated samples from the expanded network are input into the LSTM-FCN model for parallel feature extraction and information fusion, contributing to fault identification. Gao et al. [12] proposed a new approach to fault diagnosis with integrated convolutional transformer GAN (ICoT-GAN), which fully takes into account the global interactions and local dependencies of vibration signals, which is realized by incorporating the novel ICoT in the discriminator and generator, allowing the expansion to generate high-quality usable samples. Du et al. [13] proposed a combination of generative adversarial network and incremental learning SVM model for fault diagnosis, which selects sensitive features as inputs through a three-step optimal selection strategy of manual screening, relevant feature selection, and redundant feature removal, which enables adversarial learning between the generator and the discriminator to generate a small number of classes of data. Han et al. [14] introduced a semi-supervised adversarial learning network designed to efficiently address the challenge of limited labeled samples for fault identification. Qian et al. [15] proposed a novel network to reduce domain differences Relational Transfer Domain Generalization Network (RTDGN). They improved domain confusion with an inverse entropy loss and a multi-discriminator adversarial network, enhancing fault diagnosis capabilities. Moreover, Xing et al. [16] introduced a novel fault diagnosis method based on Neural Cost-sensitive Neural Networks (NCNN). In this approach, they first optimize the cost-sensitive loss function during feature extraction. Subsequently, they calculate the distance between the extracted features and the center vector for fault identification. Jiang et al. [17] used the idea of integrated learning and proposed data augmentation aiming to make data augmentation through cooperation and competition in generating data, introducing Multi-source Data Augmentation (MSDA) on the cooperation side for combining training to alleviate the problem of data skewing and designing a df-ct-MSDA method on the competition side to filter the data and thus augment the data for imbalanced data. GBSS, a novel semi-supervised learning framework proposed by Farajzadeh-Zanjani et al. [18] combines conditional generative networks with semi-supervised ladder networks and autoencoders. The generative adversarial network synthesizes a few samples, while the GBSS trains a semi-supervised model to learn the few sample distribution and iteratively adjusts its weights, effectively improving the fault diagnosis performance. Hu et al. [19] introduced an oversampling technique termed FSDA-SMOTE to generate additional fault samples. Following this augmentation, they constructed a Residual Attention Convolutional Network (RA-CNN) for fault recognition. Ruan et al. [20] proposed an improved fault diagnosis method using local weak supervision and non-local operations. This addresses low accuracy in sparse training datasets by enhancing convolutional neural networks to capture long-term dependencies during feature extraction.

The techniques above, which involve feature extraction and enhancing model accuracy, Operate within the Euclidean space data processing framework. However, in increasing

application scenarios, considering relationships and interdependencies between sample data and presenting them through graph data structures [21]. Given that graph data within non-Euclidean space inherently encapsulates substantial information about fault samples, the preceding model's approach to feature extraction and fault recognition concentrates solely on select node-specific information within the samples, which results in the model facing more significant difficulties in extracting features and thus not achieving the desired results. Graph Neural Network (GNN) [22] directs its attention toward node attribute features and edge information within the graph. Notably, specific edge information about fault features often exhibits heightened prominence; therefore, extracting fault features and improving classification accuracy is easier. GNN has found extensive application across diverse domains, including transportation [23], medicine [24], emotion recognition [25], and power systems [26]. Given their derivation from Convolutional Neural Networks (CNNs), Graph Convolutional Neural Networks (GCNs) leverage the inherent structural relationships within graphs to extract the geometric structural dependencies within the data. Li et al. [27] introduced benchmarks designed for node-level and graph-level diagnosis of mechanical faults. They subjected Graph Convolutional Networks (GCNs) to a rigorous assessment across multiple GCN variants based on frequency and spatial domains, thus substantiating the efficacy of the proposed scheme. Mo et al. [28] introduced a graph convolutional neural network that integrates a weighted horizontal visibility graph (WHVG) designed to convert vibration signals into a graph composed of visibility connections. Afterwards, a new edge weighting method is proposed to attenuate the noise interference. Despite the successful application of these models in the field of fault diagnosis, they still face a critical problem that needs to be solved: intelligent fault diagnosis requires a large amount of available monitoring data to train the models for feature extraction. However, real-world engineering environments are characterized by long uptime of mechanical equipment, resulting in a scarcity of accessible fault data. This dilemma poses a great challenge to model training, which further leads to the problem of low accuracy of intelligent fault recognition, thus creating a huge obstacle to effective fault diagnosis.

This paper proposes a new method for diagnosing faults in rotating machinery to address the issue. The one-dimensional vibration signal is initially transformed into a two-dimensional image using the Gram angle difference field technique. Concurrently, the Wasserstein Distance Gradient Penalty Generation Adversarial Network (WGAN-GP) is employed for dataset augmentation to attain data balance. Secondly, the extended image data alongside the initial image data are fed into the Convolutional Block Attention Module-Residual Network (CBAM-ResNet) architecture, facilitating the targeted extraction of feature attributes and the resultant acquisition of the feature matrix. Finally, the graph's adjacency matrix is derived by applying the GGL method, and the obtained feature matrix and adjacency matrix are fed into the graph neural network to extract the features of the graph data in depth to realize the accurate classification of rotating machinery faults. The primary contributions of this study can be summarized as follows:

(1) This study employed a novel technique to transform vibration signals into images. The method not only converts differences in one-dimensional vibration signals into two-dimensional image disparities but also retains all information about the faulty sample, ensuring no loss of information. By inputting these converted images into the WGAN-GP network proposed in this paper, high-quality usable fault samples can be generated, guaranteeing an ample dataset for training intelligent fault diagnosis models.

(2) A novel approach for constructing the feature matrix is introduced, utilizing a residual network with convolutional attention to derive the feature matrix for graph convolutional neural networks. This forms the basis for subsequent fault diagnosis.

(3) CBAM-ResNet-GCN integrates the spatial feature blocks CBAM-ResNet with the structural feature blocks GCN, facilitating a more comprehensive and efficient extraction of fault features. This effective combination makes fault diagnosis of rotating machinery much easier.

The remainder of this article is structured as follows. Section II introduces the basic concepts and contents of the Gram angle difference field, Generative Adversarial Networks, and Graph Convolutional Neural Networks. In Section IV, the network model of this paper is described in detail. Section III is specifically applied to two datasets and experimentally analyzed and discussed. In Section V, some conclusions drawn from this paper are summarized.

II. THEORETICAL BACKGROUND

A. GRAM ANGLE DIFFERENCE FIELD

To fully harness the information within one-dimensional vibration signals and underscore the potent capabilities of generative adversarial networks in handling image data, this paper employs a novel approach: the conversion of one-dimensional (1D) vibration signals into a novel time series of two-dimensional (2D) images, achieved through the application of the Gram angle difference field technique [29]. The procedure for constructing the Gram angle difference field is delineated as follows:

1) Initially, the set of n time series vibration signals $X = \{x_1, x_2, \cdots, x_n\}$ is subjected to rescaling within the range of and subsequent normalization. The mathematical expression for this operation is provided as follows:

$$\widehat{x}^i = \frac{[x_i - \max(X)] + [x_i - \min(X)]}{\max(X) - \min(X)} \tag{1}$$

2) After normalization, the timestamp is encoded as a radius by encoding the value as an inverse cosine function, as follows:

$$\begin{cases} \alpha_i = \arccos\theta\left(\hat{x}^i\right), -1 \le \hat{x}^i \le 1, \hat{x}^i \in \tilde{X} \\ r_i = \dfrac{t_i}{N}, t_i \in N \end{cases} \tag{2}$$

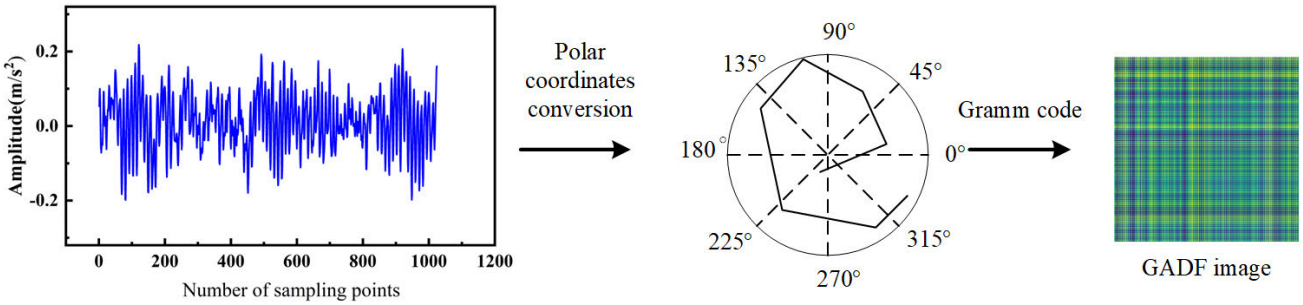

FIGURE 1. Schematic diagram of the conversion of a vibration signal into a gram angle difference field (GADF).

where the time series $\tilde{X}$ represents the rescale sequence within the polar coordinates; t_i represents the timestamp; N represents the factor determining the radial span. This novelty approach utilizes polar coordinate systems to visualize time series. Over time, the corresponding $\tilde{X}$ time series is projected onto polar coordinates, producing curvature between different angles along the circumference, as shown in Fig. 1.

3) The GADF matrix is obtained from the GAF based on the difference operation of the sinusoidal function, as follows:

$$\begin{aligned} GADF_{(i,j)} &= \left[\sin\left(\alpha_i - \alpha_j\right)\right] \\ &= \begin{bmatrix} \sin\left(\alpha_1 - \alpha_1\right) & \cdots & \sin\left(\alpha_1 - \alpha_n\right) \\ \vdots & \ddots & \vdots \\ \sin\left(\alpha_n - \alpha_1\right) & \cdots & \sin\left(\alpha_n - \alpha_n\right) \end{bmatrix} \\ &= \sqrt{I - \tilde{X}'^2} \cdot \tilde{X} - \tilde{X}' \cdot \sqrt{I - \tilde{X}^2} \end{aligned} \tag{3}$$

where $GADF_{(i,j)}$ represents the image generation matrix associated with Gram's angular difference field; I represent the unit row vector. Following the conversion, the initial time series can undergo a metamorphosis into a diagonally symmetric Gram matrix, which is then converted to a two-dimensional image.

B. WGAN-GP

Generative Adversarial Networks (GANs) primarily generate information about the features of similar samples by learning from the features of data in the original samples, facilitating data enrichment.

The limited control of GAN networks over generators can lead to training instability and model breakdown. To address this, Arjovsky et al. [30] introduced WGAN (Wasserstein Generative Adversarial Network, WGAN) as a solution to these shortcomings. The optimization objective function for WGAN is as follows:

$$W\left(p, q\right) = \inf_{r \sim \pi(p,q)} E_{(\tilde{x},\tilde{y})\sim r}\left[\| \tilde{x} - \tilde{y} \|\right] \tag{4}$$

where $\pi\left(p, q\right)$ represents the joint distribution of p, q; $(\tilde{x}, \tilde{y})$ represents samples from the joint distribution r; $E_{(\tilde{x},\tilde{y})\sim r}\left[\| \tilde{x} - \tilde{y} \|\right]$ represents the expectation of the distance $\left[\| \tilde{x} - \tilde{y} \|\right]$; $\inf(\cdot)$ represents the lower bound of the set; $W\left(p, q\right)$ represents the Wasserstein distance of the two distributions.

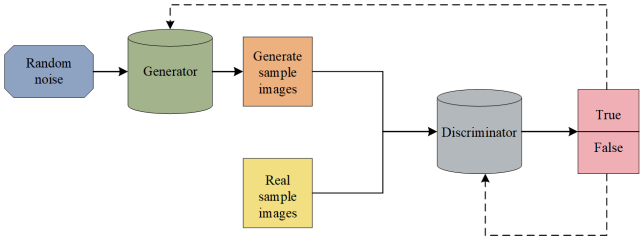

FIGURE 2. Schematic diagram of WGAN-GP structure.

Incorporating the gradient penalty strategy onto the foundation of WGAN enables optimization of the WGAN intercept [31]. This alteration steers the Loss towards an idealized trajectory, resolving convergence challenges. The resultant optimized objective loss function is as follows:

$$\begin{aligned} D_{loss} = {} & E_{x_r \sim P_g}\left[D\left(x_r\right)\right] - E_{x_f \sim P_g}\left[D\left(x_f\right)\right] \\ & - \mu E_{\hat{x} \sim P_{\hat{x}}}\left[\left(\| \nabla_{\hat{x}} D\left(\hat{x}\right) \|_2 - 1\right)^2\right] \end{aligned} \tag{5}$$

where $x_r \sim P_g$ represents distribution for real data, $x_f \sim P_g$ represents generating data distribution of data; μ represents the penalty coefficient; $\hat{x}$ represents the linear difference between x_r and x_f; D_{loss} represents the discriminator loss.

In this study, the Adam optimizer is employed for parameter update in the expanded model, utilizing a learning rate of 0.0001 and a batch size of 32. The WGAN-GP undergoes training through 10,000 iterations. Within each iteration, the generator is executed once, while the discriminator is executed six times, both undergoing iterative updates. The objective of the generator is to generate a 256 × 256 image. It takes a 100-dimensional noise vector as input and features a network architecture comprising a single fully connected layer and six inverse convolutional layers. The fully connected layer contains 1024 neurons, while each inverse convolutional layer employs a 4 × 4 filter with a stride of 2. The layer-by-layer convolutional kernels are configured as follows: 512, 256, 128, 64, and 32. The chosen activation function is ReLU. The discriminator network comprises multiple layers, encompassing three convolutional layers and a fully connected layer. In the convolutional layers, 5 × 5 kernels are applied with a stride of 2 for each layer. The convolutional kernels progressively increase: 256, 512, and 1024. The fully connected layer hosts a single neuron, employing

LeakyReLU as the activation function. The architecture of the WGAN-GP used in this study is shown in Fig. 2.

C. GRAPH CONVOLUTIONAL NEURAL NETWORKS

Graph convolution networks [32] can be classified into two categories: spatial domain graph convolution and frequency domain graph convolution. The former involves performing convolution operations directly on the graph nodes, yielding rapid computational speed albeit with relatively limited theoretical grounding. On the other hand, the latter entails frequency domain graph convolution achieved through Laplace eigen-spectrum decomposition. This approach offers mathematical interpretability and theoretical underpinnings. Thus, this study employs the spectral domain graph convolution method for unfolding.

The graph can be represented as $G = G(V, E, A)$, where V represents a node, E represents the set of edges, and A represents the graph's adjacency matrix. For an undirected graph, A_{ij} represents the connection between two nodes V_i and V_j, which is represented as 1 in the adjacency matrix if an edge exists and 0 otherwise, as follows:

$$A_{ij} = \begin{cases} 1, if \exists \left(V_i, V_j\right) \in E \\ 0, otherwise \end{cases} \tag{6}$$

The graph can also be expressed as $L = D - A$, where $D_{ii} = \sum_j A_{ij}$, with L representing the Laplace matrix and D representing the degree matrix. The symmetric normalized Laplace matrix is usually used, as follows:

$$L^{sym} = I_N - D^{-1/2} A D^{-1/2} = U \Lambda U^T \tag{7}$$

where L^{sym} represents the symmetrically normalized matrix; I_N represents the unit matrix; $U = (u_1, u_2, \cdots, u_n)$ represents a matrix composed of unit eigenvectors; Λ represents the diagonal matrix comprising the n eigenvalues of the Laplace matrix.

The filter used in the graph convolution is $g_\phi = diag\left(U^T g\right)$, the computation between the graph signal f and the convolution kernel g is as follows:

$$f * g = U \begin{pmatrix} \hat{g}(\lambda_1) & \cdots & 0 \\ \vdots & \ddots & \vdots \\ 0 & \cdots & \hat{g}(\lambda_n) \end{pmatrix} U^T f \tag{8}$$

To alleviate the computational burden of graph convolution, the convolution kernel $\hat{g}(\Lambda)$ can be approximated using the kth-order expansion of the Chebyshev polynomial $T_k(\cdot)$. This approximation is represented by:

$$\hat{g}(\Lambda) \approx \sum_{k=0}^{K-1} \theta_k T_k\left(\tilde{\Lambda}\right) \tag{9}$$

where θ_k represents the Chebyshev factor. Notice that $UT_k\left(\tilde{\Lambda}\right)U^T = T_k\left(U\tilde{\Lambda}U^T\right)$ is easily shown to hold. Moreover, $\theta = \theta_0 = -\theta_1$ is assumed, strategically restricting the number of parameters to mitigate overfitting. Given these considerations, the definition of graph convolution can be effectively approximated by:

$$f * g = \theta\left(\tilde{D}^{-1/2}\tilde{A}\tilde{D}^{-1/2}\right)f \tag{10}$$

where $\tilde{A} = A + I_N$ considers its own properties for the adjacency matrix A. The propagation rule for the convolutional layer in GCN is as follows:

$$H^{(l+1)} = \sigma\left(\hat{A}H^{(l)}W^{(l)}\right) \tag{11}$$

where W represents the matrix of learnable parameters; $H^{(l)}$ represents the node features in layer l; $\sigma(\cdot)$ represents the activation function; $\hat{A}$ represents the updated adjacency matrix, and $\hat{A} = \tilde{D}^{-1/2}\tilde{A}\tilde{D}^{-1/2}$ signifies its normalization to both the left and right of $\tilde{A}$.

The graph convolution concept is illustrated in Fig. 3, wherein the update of a new node includes the sum of the neighboring feature information multiplied by their corresponding weights and the intrinsic attributes of the node. This aligns with the formula (12). Fig. 4 depicts a two-layer standard Graph Convolutional Network (GCN), and node classification is obtained after the classifier.

$$\begin{cases} h_1' = h_1 + h_e W \\ h_e = h_2 + h_3 + h_4 + h_5 + h_6 \end{cases} \tag{12}$$

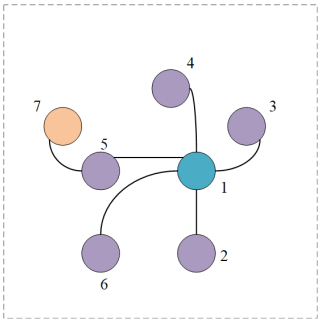

FIGURE 3. Graph convolutional schematic.

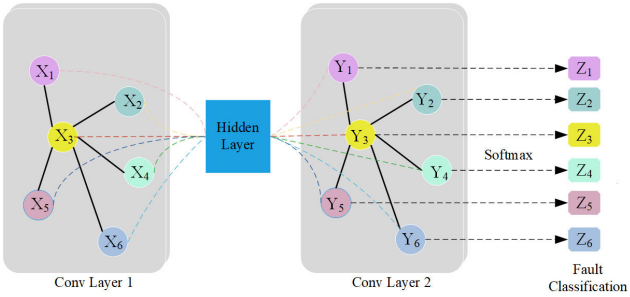

FIGURE 4. Two-layer standard graph convolutional model.

III. PROPOSED METHOD

A. DATA PREPROCESSING AND AUGMENTATION

This paper's data preprocessing and augmentation module consists of two main components. The first part primarily addresses the issue of insufficiently extracted information from one-dimensional vibration signals. It employs a novel

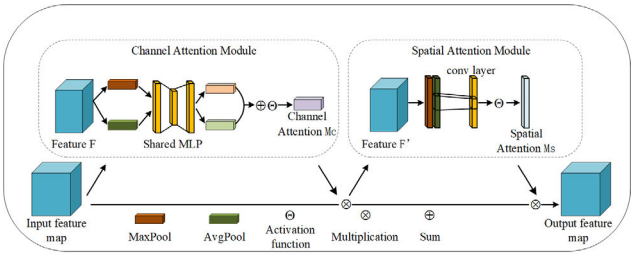

FIGURE 5. Schematic diagram of CBAM attention module.

time series method called Gram angle difference field to convert them into two-dimensional images. The second part expands the dataset using a WGAN-GP network, ensuring a balance between the number of faulty samples in each category and the number of normal samples while maintaining the quality of the generated images.

B. FEATURE EXTRACTION

The feature extraction process in this study predominantly composed of two primary components: the spatial feature block and the structural feature block. GCN excels in handling data within non-Euclidean spaces adeptly. Its GCN operation necessitates inputs such as the adjacency matrix and the feature matrix and exhibits a degree of interpretability. For the acquisition of the node feature matrix, this paper employs CBAM-ResNet for feature extraction.

1) Spatial feature blocks: Effective feature extraction can substantially enhance classification outcomes. This study employs a residual network enriched with a convolutional attention mechanism known as CBAM-ResNet. This architecture is built upon ResNet while incorporating CBAM modules [33]. Introducing CBAM modules enables focused attention on crucial features, diminishing operation complexity. The network encompasses four residual modules. Each residual block comprises four convolutions using a 3×3 convolutional kernel at a stride of 1. Post convolution, batch normalization (BN) is applied to mitigate internal covariance bias. The ReLU activation function expedites model convergence and enhances feature segmentation. Additionally, the model integrates a global maximum pooling layer and an average pooling layer with a pooling size of 2×2 and a stride of 2. Furthermore, two attentional convolution modules are embedded after the respective pooling layers. The CBAM module is introduced into ResNet, as depicted in Fig. 5 below. This module is comprised of two primary components. The first component is the channel attention module, which fundamentally fuses spatial information within the feature map via two pooling operations, computed as follows:

$$M_C(F) = \sigma\left(MLP\left(AvgPool\left(F\right)\right) + MLP\left(MaxPool\left(F\right)\right)\right) \tag{13}$$

The remaining component is the spatial attention module, gathering feature map information along the channel direction to yield two maps. Subsequently, these maps are concatenated and subjected to convolution through a standard convolutional layer, generating the 2D spatial attention map, computed as follows:

$$M_S(F) = \sigma\left(f^{7\times7}\left(\left[AvgPool\left(F'\right); MaxPool\left(F'\right)\right]\right)\right) \tag{14}$$

where σ is the activation function; $f^{7\times7}$ is convolutional kernel operation of size 7×7.

CBAM-ResNet extracts and acquires features from the feature graph, with each feature vector representing a node and its corresponding value representing a node feature. The fully connected layer fine-tunes the CBAM-ResNet output to conform to the graph's convolutional input structure. Consequently, the output of each small batch of input CBAM-ResNet is as follows:

$$\chi = CBAM - \mathrm{Re}sNet\left(X_{input}\right) \tag{15}$$

where X_{input} represents the small batch input matrix, and χ represents the feature matrix of the node.

2) Structural feature blocks: The graph construction methodology employs the Graph Generation Layer (GGL) [34] to establish a fault sample graph. Following the collection of spatial features by CBAM-ResNet, the adjacency matrix is calculated as follows:

$$A = normalize\left(\tilde{\chi}\,\tilde{\chi}^T\right) \tag{16}$$

where $\tilde{\chi}$ represents the node feature after the multilayer perceptron, this feature is subjected to matrix multiplication with its transposed counterpart to yield the adjacency matrix A, while $normalize\,(\cdot)$ signifies the normalization function. To alleviate the computational burden, the acquired adjacency matrix A is transformed into a sparse matrix as follows:

$$\breve{A} = Top - \kappa\,(A) \tag{17}$$

where $\breve{A}$ represents the sparse matrix; $Top - \kappa\,(\cdot)$ represents the index of the first κ maxima of A returned.

The generated fault sample map is fed into the proposed two-layer GCN for depth extraction of features. However, a challenge arises: the weights between nodes are different. Some researchers, aiming to simplify the issue, assume uniformity across nodes. In addition, specific individuals advocate directly setting $W_{ij} = A_{ij}$, treating the adjacency matrix as the weight matrix. Consequently, weights become 0 or 1, inducing drastic weight alterations that impact classification accuracy. Moreover, this approach fails to embody graph neural networks' robust feature extraction capability. Hence, this study employs the Gaussian kernel function to compute assigned edge weights. This function offers sound interpretability and is calculated as follows:

$$W_{ij} = \exp\left(-\frac{d\left(\psi_i, \psi_j\right)^2}{2\vartheta}\right) \tag{18}$$

where W_{ij} represents a weight parameter ranging from $0 \leq W_{ij} \leq 1$; $d\left(\psi_i, \psi_j\right)$ represents a distance metric; ϑ represents the bandwidth variance of the Gaussian kernel function.

To enhance the nonlinear representation capability during aggregation and counteract overfitting, this study adopts the

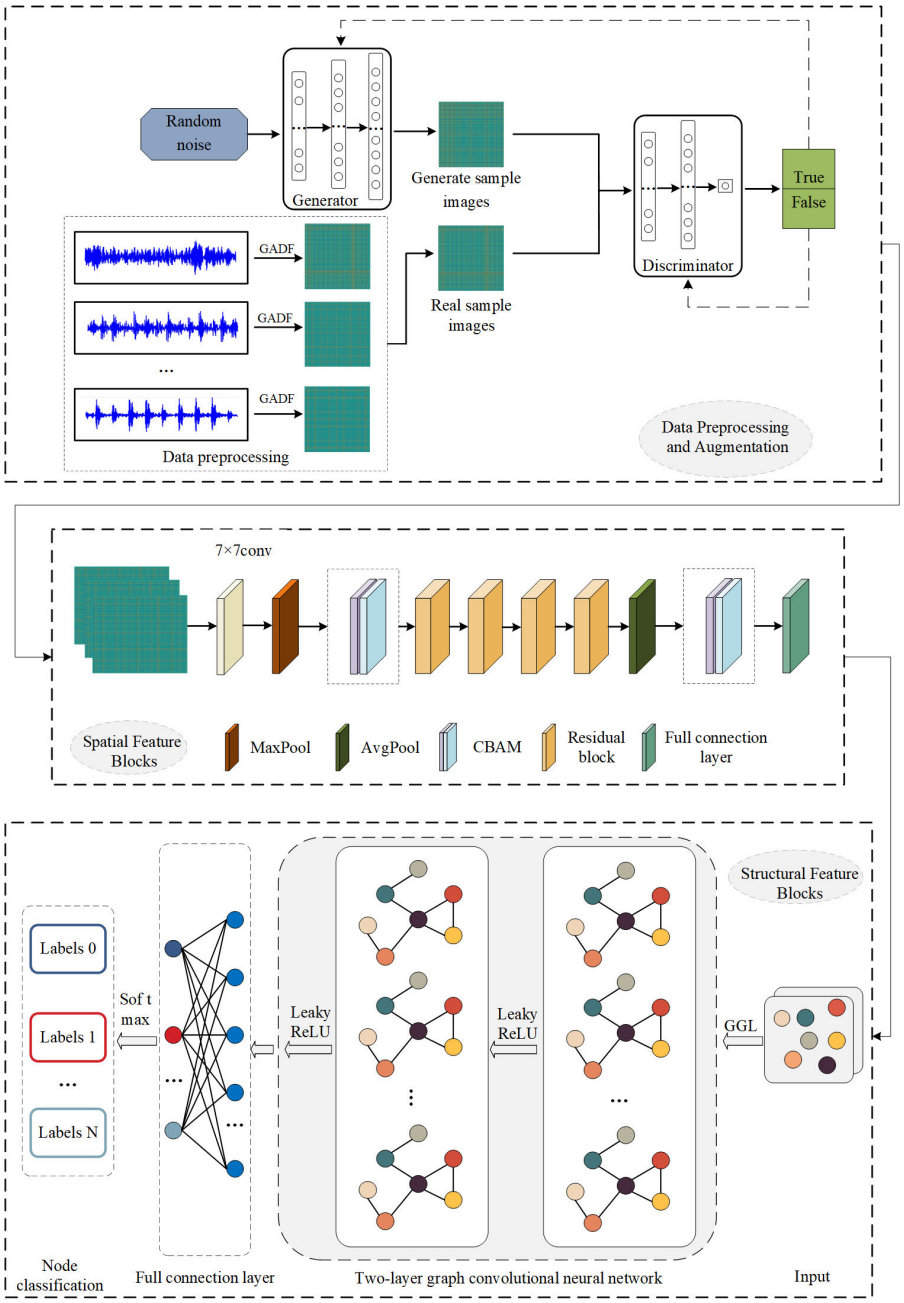

FIGURE 6. General framework diagram of the proposed fault diagnosis method.

Leaky Rectified Linear Unit (LeakyReLU) as the activation function. The GCN model consists of two Chebyshev graph convolution layers, two LeakyReLU activation layers, and a SoftMax layer. In each graph convolution layer, the model adaptively captures high-dimensional information from the input data. The predictive label formulation for the GCN model is as follows:

$$Z = Soft\max\left(\breve{A}Leaky\mathrm{ReLU}\left(\breve{A}\chi W^{(1)}\right)W^{(2)}\right) \tag{19}$$

where $W^{(i)}$ represents the trainable weight matrix; Z represents the sample's label.

In the model employed within this study, the cross-entropy loss function for the samples serves as the optimization criterion, and weight parameters are updated via backpropagation. Subsequently, a Dropout layer is introduced to mitigate the impact of overfitting. The loss function is expressed as follows:

$$LF = -\sum_{i\in V_{label}}\sum_{j=1}^{F} Y_{ij}^{r}\ln\left(Y_{ij}^{P}\right) \tag{20}$$

where Y_{ij}^{r} represents the real label of the ith-labeled node; Y_{ij}^{P} represents the predicted label of the ith-labeled node; V_{label} represents the set of labeled nodes.

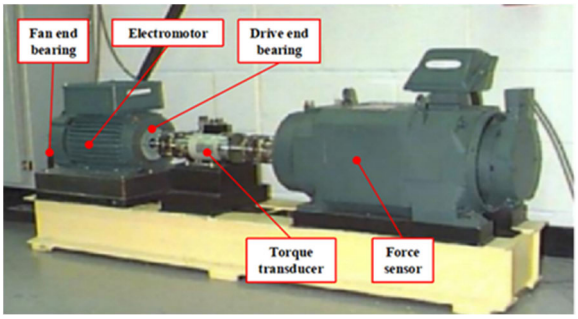

FIGURE 7. Case western reserve university fault data acquisition test rig.

The fault diagnosis model proposed in this paper is illustrated in Fig. 6. First, the collected vibration signals undergo conversion into images via the Gram angle difference field and utilizing WGAN-GP to Generate High-Quality Sufficient Training Sets. Following this, the image samples are fed into CBAM-ResNet to extract feature attributes, yielding the feature matrix. Lastly, a graph generation layer is employed to establish the fault sample graph and derive the adjacency matrix. The obtained feature matrix and adjacency matrix are then input into the constructed two-layer GCN for deep feature extraction among samples and their edge information features. Finally, a softmax classifier accurately categorizes the faults.

IV. EXPERIMENTS AND DISCUSSION

The hardware configuration for the experiments conducted in this study is specified as follows: Windows 10 operating system, NVIDIA GTX3070 graphics card for GPU, Inter-i5 for CPU, and the program is implemented by Pytorch and Pytorch_geometric framework. The model was trained with a learning rate 0.0001, using the Adam optimizer with a cross-entropy loss function and 50 iterations. To prevent overfitting of the model, the Dropout layer was set to have a dropout rate of 0.2. Finally, the Softmax classification function is used to classify the fault types.

A. CASE WESTERN RESERVE UNIVERSITY DATASET

The CWRU bearing dataset has four different operating conditions: 0 load at 1797 rpm, 1 load at 1772 rpm, 2 load at 1750 rpm, and 3 load at 1730 rpm. In all scenarios, bearing failures manifest as inner ring failures, ball faults, and outer ring faults. Each of these can be further classified with diameters of 0.007, 0.014, and 0.021 inches, contingent upon the extent of damage. These three fault categories collectively form a 10-class classification task in conjunction with normal states. Throughout the experiments, uniform testing conditions were maintained. In this study, experimental data from SKF's 6205 deep groove ball bearing located at the driving end were utilized, and the data encompassed vibration signals recorded under conditions of a 12 kHz sampling frequency. In this paper, the length of a single sample is chosen to be 1024 points. As shown in Fig. 7, the experimental setup comprises a torque transducer, a 2-hp motor, and a dynamometer.

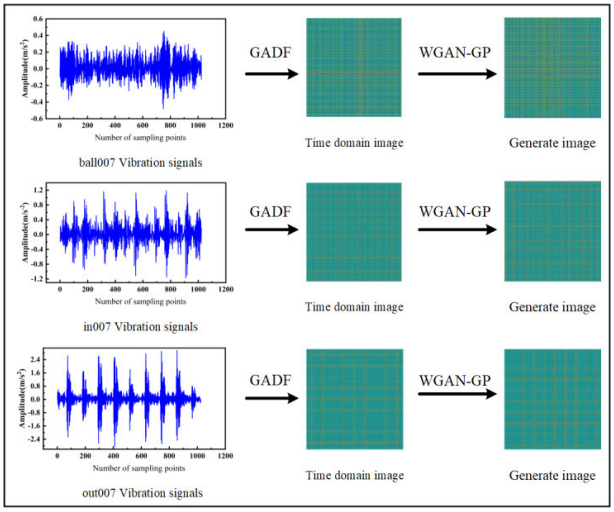

FIGURE 8. Vibration signal—gram angle difference field image—WGAN-GP generated image.

1) Construction of the Dataset: Collecting information on faulty bearings becomes more challenging due to prolonged operation under normal conditions. Therefore, this paper uses artificially set up-unbalanced datasets A, B, and C, with imbalance ratios of 1:2, 1:4, and 1:8, respectively. Table 1 shows the detailed parameters.

2) Data Preprocessing and Augmentation: Since the acquired vibration signals are one-dimensional, in this paper, the Gram angle difference field is used to convert the acquired one-dimensional vibration signals, and the one-dimensional vibration signals of the samples are converted into two-dimensional images. Data augmentation is to expand the faulty sample so that it is balanced with the number of normal samples, and the converted two-dimensional image is expanded by using WGAN-GP so that the data can be guaranteed to be sufficiently available. To facilitate visual representation, fault states corresponding to 007 inches in the inner ring, outer ring, and rolling body categories are selected for display. The resulting is shown in Fig. 8, showcasing the process of vibration signal-Gram angle difference field conversion and the expanded images achieved through WGAN-GP.

3) Model Feasibility Verification: To assess the effectiveness of the Gram's angle difference field, another variant known as the Gram's angle sum field (GASF) [35] is employed for comparison alongside the commonly utilized two-dimensional grayscale maps [36]. They are both chosen because the conversion of a one-dimensional vibration signal into an image does not require tedious calculations and selection of correlation functions, but only the consideration of the respective corresponding matrices. Specifically, three after augmentation are taken as inputs for the CBAM-ResNet-GCN model. This process is executed using dataset A under 0 operating conditions, and the accuracy and loss of fault diagnosis are depicted in Fig 9.

In this figure, the left scale indicates the fault identification accuracy and the right scale indicates the loss value. The

TABLE 1. Description of case western reserve university rolling bearing failure dataset.

Fault label	Damage state	Training set A	Training set B	Training set C	Val/Test set
0	ball007	700	350	175	400/200
1	ball014	700	350	175	400/200
2	ball021	700	350	175	400/200
3	in007	700	350	175	400/200
4	in014	700	350	175	400/200
5	in021	700	350	175	400/200
6	normal	1400	1400	1400	400/200
7	out007	700	350	175	400/200
8	out014	700	350	175	400/200
9	out021	700	350	175	400/200

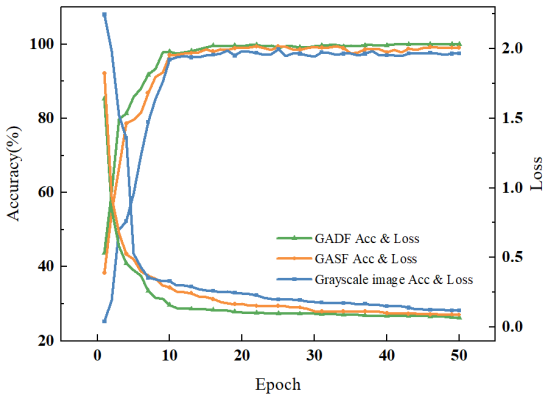

FIGURE 9. Accuracy and loss plots with different images as inputs.

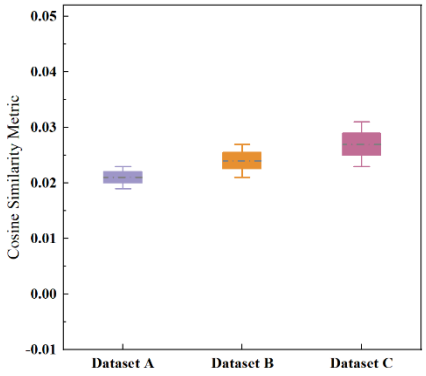

FIGURE 10. Box-plot on three datasets.

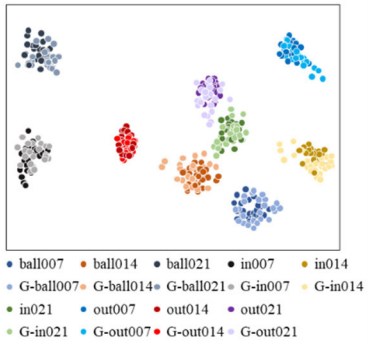

FIGURE 11. Visualization of real samples vs. generated samples.

figure reveals that the proposed model achieves an accuracy exceeding 97% when three different images ways are used as inputs. The loss value decreases smoothly, indicating a strong fitting ability of the model. Notably, when GADF is used as input, the model converges rapidly, achieving slightly higher accuracy compared to the other two approaches by about 0.5-1.5%, and the loss is minimized. This rapid convergence and high accuracy demonstrate the stability of the model during training, validating the feasibility and effectiveness of using GADF in this paper.

The synthesized samples are evaluated through various measures to assess the quality of the WGAN-GP generated samples adopted in this study. Firstly, it is evident from the figure above that the expanded image is not a mere copy of the pre-expanded version; instead, it exhibits slight differences. This observation underscores the diversity inherent in the generated samples. The cosine similarity metric is employed further to affirm the validity and authenticity of these generated samples [37]. The vertical coordinate in Fig. 10 represents the cosine similarity measure; The smaller the value of this metric, the greater the similarity between the compared samples, which means that the gap between the samples is small.

Fig. 10 presents a box plot depicting the statistical metrics comparison between the generated and original samples across the three datasets. In this plot, the dotted line represents the mean. Samples further away from the mean line exhibit more significant fluctuation and poorer quality. As can be seen, the three data set metrics are minimal, indicating a preferable generation effect that meets the requirements of the training model. It is worth noting that the smallest value of this metric in the three datasets is in dataset A, which indicates that the image samples generated in dataset A are better than those in B and C. The value of this metric in dataset A is the lowest. This is due to the fact that as the imbalance ratio increases, the more scarce the raw data becomes. Thus dataset A becomes the best choice among the three.

Furthermore, for a more comprehensive image quality assessment, t-SNE [38] is employed to visualize the similarity between the generated and original data. This visualization focuses on the 9 types of samples generated in dataset A. The more similar the generated data are to the original data, the more they will be clustered together, otherwise they will be discrete, as shown in Fig. 11. The results illustrate that the 9 classes of generated samples cluster with their

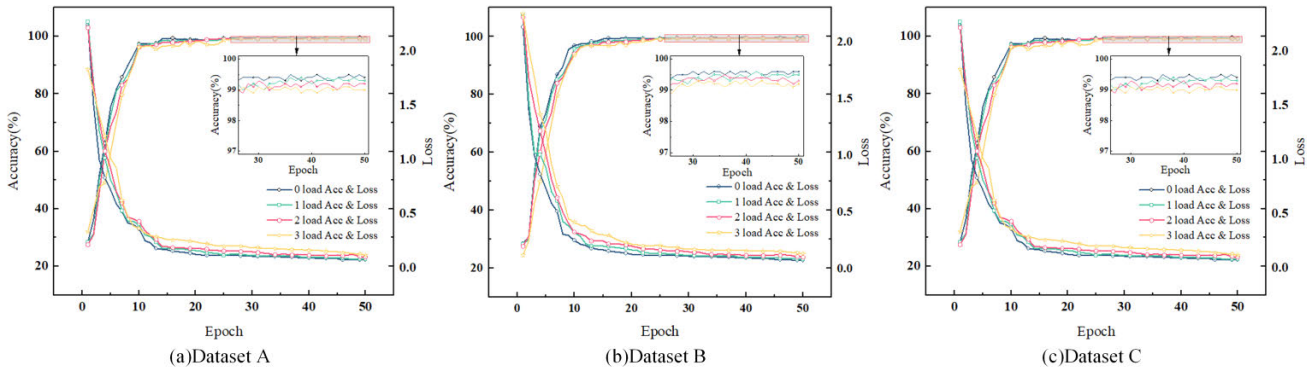

FIGURE 12. Test accuracy and loss curves for three datasets under four different operating conditions.

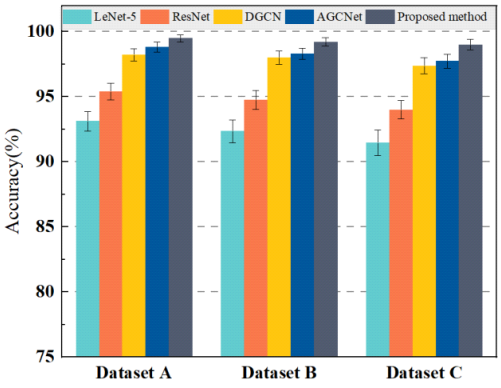

FIGURE 13. Plot of fault recognition accuracy of different models on three datasets.

corresponding real samples. Only extremely rare generated samples were not correctly clustered, underscoring the high quality and effectiveness of the generated samples.

To validate the performance of the proposed model, experiments were conducted using three datasets under four different operating conditions. The results of these tests are shown in Fig. 12.

The results demonstrate that the model attains approximately 99% accuracy across four distinct operating conditions in all three unbalanced datasets. The losses consistently decrease without any signs of overfitting. The accuracy rate exhibits a smooth increase after the tenth iteration, reaching close to 97%, highlighting the rapid convergence capability of the proposed model. Fig. 12 illustrates that dataset A exhibits a higher accuracy rate than B and C with a smoother curve. This difference may be attributed to the increased imbalance ratio in the latter two datasets. While the expanded image may not be a perfect replica of the original, this factor is negligible compared to the impact of unbalanced data on diagnostic accuracy.

4) Comparison Experiments With Other Deep Learning Methods: This paper will conduct comparative experiments with several other models to assess the efficacy of the designed CBAM-ResNet-GCN model in addressing the task of rotating machinery fault diagnosis. These models include Deep Convolutional Neural Network (LeNet-5) [39],

TABLE 2. Average accuracy of each model under three unbalanced dataset.

Methods	Mean accuracy±standard deviation(%)		
	Dataset A	Dataset B	Dataset C
LeNet-5	93.124±0.758	92.345±0.856	91.469±0.986
ResNet	95.394±0.632	94.756±0.721	94.003±0.698
DGCN	98.218±0.469	98.008±0.512	97.386±0.635
AGCNet	98.817±0.381	98.306±0.436	97.745±0.527
Proposed method	99.487±0.270	99.229±0.331	99.006±0.412

Residual Neural Network (ResNet) [40], DGCN [41], and AGCNet [42] for fault diagnosis. The former two models are non-graph structures, while the latter two models are GCN-based. The models are trained using uniform hyperparameter settings and initialization methods. To ensure the reliability of the experiments, each set of experiments is repeated ten times, and the results are averaged to provide outcomes. A summary of the outcomes for various methods is presented in Table 2, and the test results are shown in Fig. 13.

From the results, it can be seen that two traditional CNN-based methods; LeNet-5 and ResNet, performed poorly in each experiment. Attributed to the fact that these two models lack graph structure and are data-driven based, with limited training data, these models are unable to reach their full potential and may suffer from overfitting phenomenon, resulting in poor recognition of fault information, hence their poor performance. On the contrary, DGCN, AGCNet and the method proposed in this paper are built on graph structure models.GCN captures the dependencies between time series from the perspective of graph topology, which makes them capable of learning and extracting the feature information of the nodes and capturing the important information of the edges between the nodes. The latter three models are significantly more accurate compared to the above two models. The reason why the model proposed in this paper outperforms the other two GCN models is, on the one hand, that the CBAM attention mechanism in the spatial feature block allows targeted information extraction and reduces the interference of irrelevant information. On the other hand, the construction method of the graph data directly determines the quality of the graph data, and thus it is crucial to ensure high-quality fault sample graphs. In this paper,

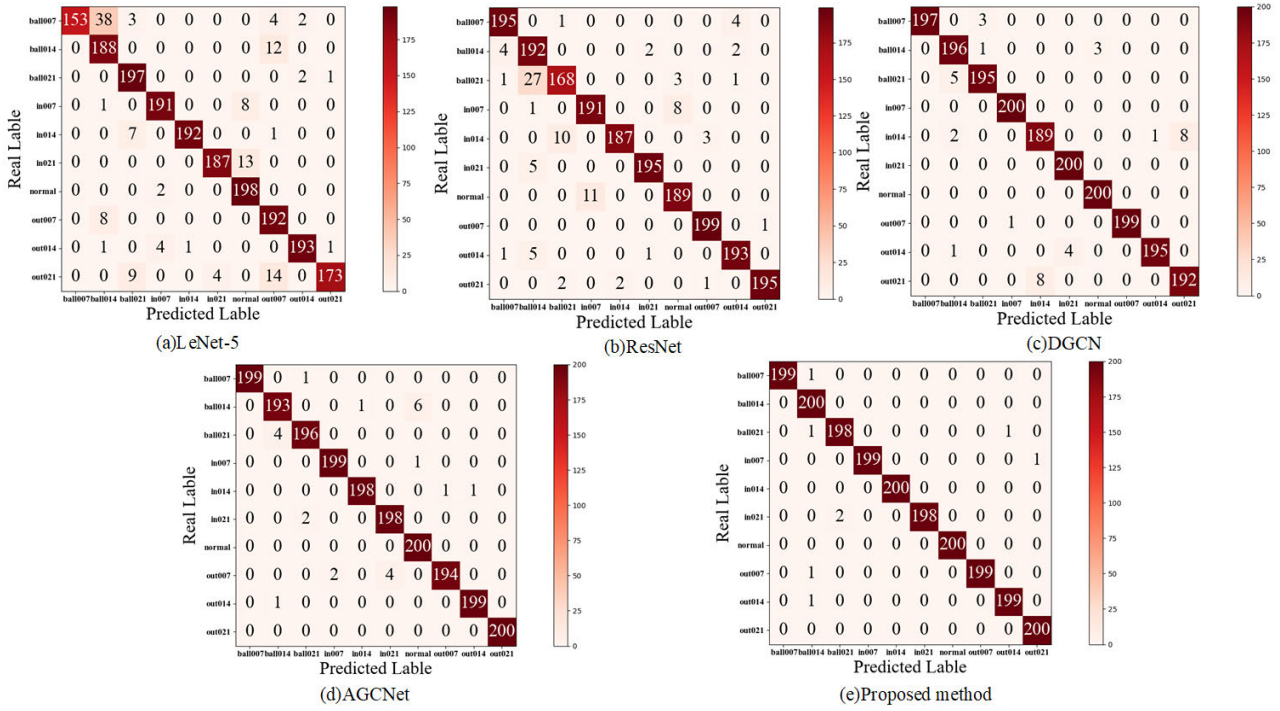

FIGURE 14. Confusion matrix plot of different models on dataset A.

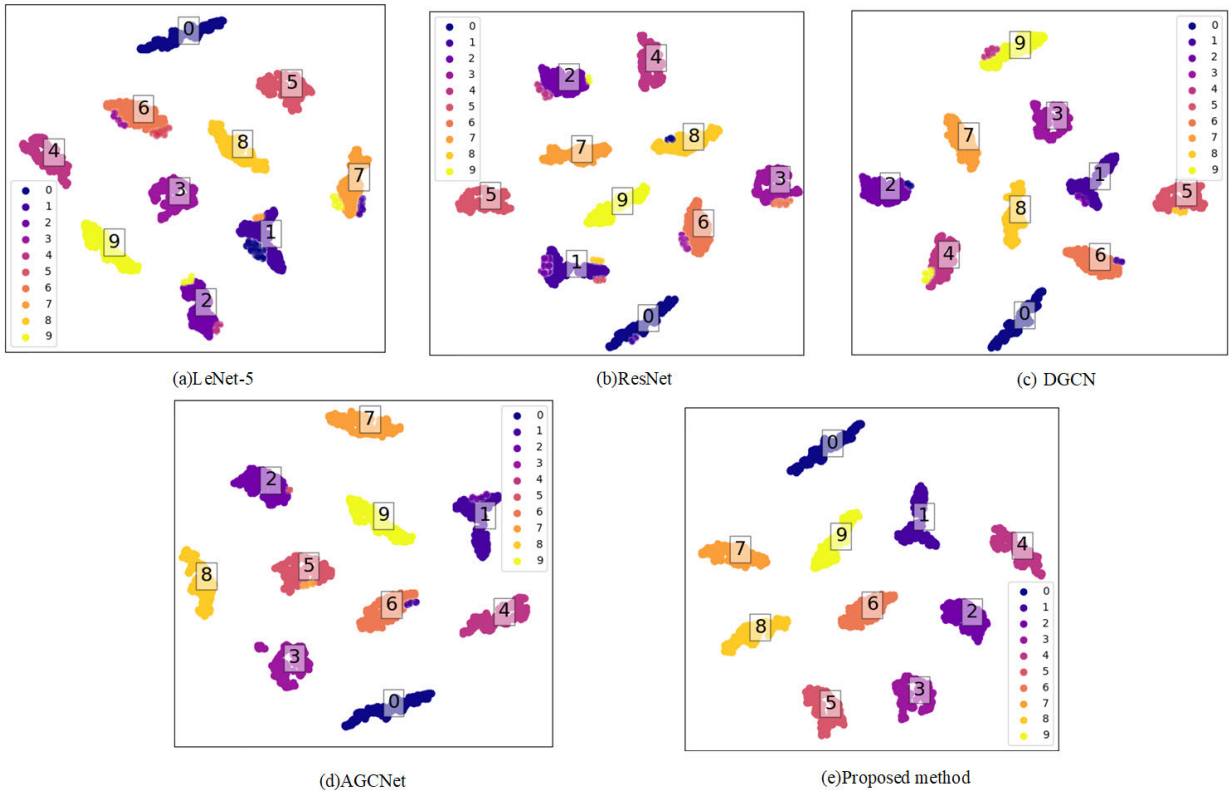

FIGURE 15. Visualization of the results of different models on dataset A.

the residual network containing a convolutional attention mechanism is used to obtain the feature matrix of GCN to construct high-quality fault sample graphs, which makes Enables structural feature blocks to better identify faults. As can be seen from Table 2, the standard deviation of this paper is smaller than the other four models, which further

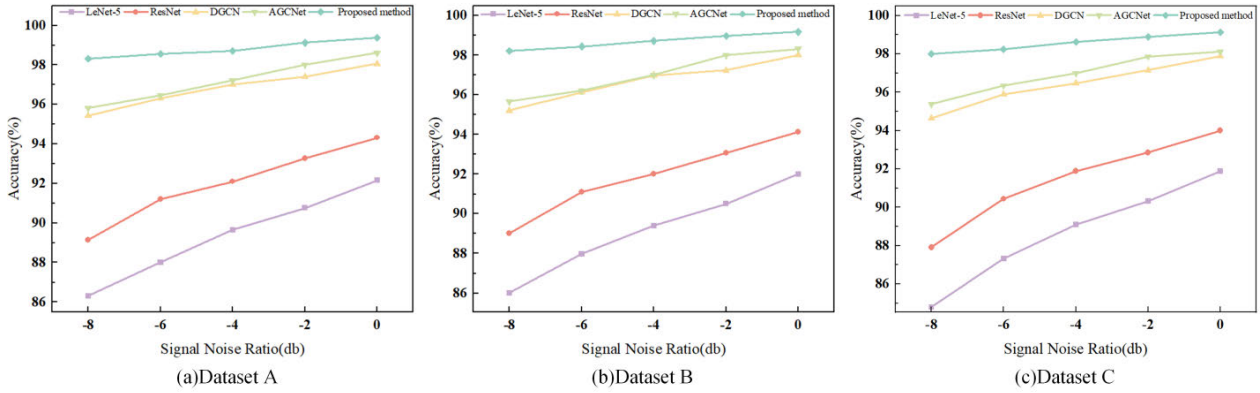

FIGURE 16. Comparison of fault recognition accuracy for different signal-to-noise ratios on three datasets.

indicates the better stability of the method proposed in this paper.

To intuitively compare the performance of the model proposed in this paper with four other models in terms of diagnosing faults in rotating machinery, this study analyzes the model's output characteristics under dataset A using a confusion matrix and visualization techniques. The confusion matrix is shown in Fig. 14, and the visualization results are shown in Fig. 15.

From Fig. 14, one can get the following observations: LeNet-5, 38 samples labeled as 0 were erroneously categorized as 1. Additionally, there are more misclassifications of samples labeled 1 and 9. In the case of ResNet, 27 samples labeled as 2 were inaccurately categorized as 1, and some of the defective samples labeled as 8 were also misclassified. On the other hand, the latter three GCN-based models demonstrate a superior ability to classify each fault type from a holistic perspective accurately. DGCN and AGCNet exhibit few misclassifications, whereas the model proposed in this paper showcases an even smaller number of misclassifications. This model proves its proficiency in accurately identifying all fault types compared to the other four models.

5) Noise Robustness of the Proposed Methods: Rotating machinery often operates in complex environments and is subjected to strong noise and unbalanced data, which can lead to a decline in model performance. To verify the relevant performance of the model presented in this paper, strong noises with varying signal-to-noise ratios are exclusively added to the test sets of the three datasets. Specifically, noise of 0, -2, -4, -6, and -8 dB are introduced to the test samples of vibration signals using MATLAB's signal-to-noise function to emulate diverse noise environments encountered in engineering. Each sample comprises 1024 points and faulty samples' preprocessing and augmentation steps remain consistent with the abovementioned process. Comparative experiments are conducted across three unbalanced datasets and different noises. These experiments are repeated five times to compute an average and mitigate the influence of random factors and conditions. The outcomes are shown in Fig. 16

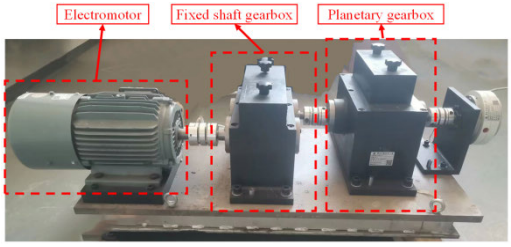

FIGURE 17. Laboratory planetary gearbox fault data test rig.

As observed in Fig. 16, the proposed model can maintain high diagnostic accuracy and training stability even in the presence of significant noise. This suggests its ability to effectively capture valid information within the samples and resist noise interference. However, as the imbalance ratio increases, there is a marginal decrease in accuracy. The proposed model achieves average accuracies of 98.324%, 98.227%, and 98.003% on the three unbalanced datasets under -8 dB strong noise. In addition, it can be seen from the Fig. 16 that all four fault diagnosis models are not as effective as the method proposed in this paper. The main reason may be that the data expansion makes the generator more resistant to the input noise. This may result in the generator producing samples that are more robust and less susceptible to noise as well as the CBAM attention mechanism focusing on feature extraction under noisy conditions. The validation results affirm the applicability of the fault diagnosis method proposed in this paper across diverse noise environments.

B. LABORATORY PLANETARY GEARBOX DATASET

Gearbox diagnosis of faults in unbalanced datasets and noise environments remains a challenge. To solve this problem, To solve this problem, in this paper use the planetary gearbox dataset tested by our research team to validate the proposed network model and verify its applicability further. The experimental setup is shown in Fig. 17 and includes an AC asynchronous motor, a fixed shaft gearbox, a planetary gearbox, and a magnetic particle brake. The first stage of the stator gearbox has 77 teeth and 55 teeth, while the second stage of

TABLE 3. Description of planetary gearbox failure dataset.

Fault label	Damage state	Training set A	Training set B	Training set C	Val/Test set
0	normal	1400	1400	1400	400/200
1	broken	700	350	175	400/200
2	crack	700	350	175	400/200

TABLE 4. Average accuracy of planetary gearbox experiments on three datasets.

Data types	Training set A	Training set B	Training set C
Proposed method	99.119	98.578	98.128

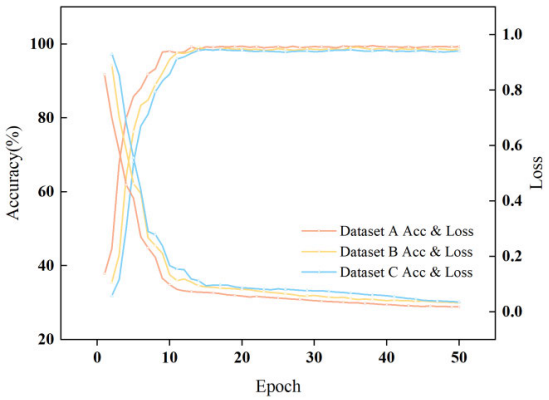

FIGURE 18. Accuracy and loss curves for gearbox experiments on three datasets.

the planetary gearbox consists of a sun wheel, a planetary gear, and a ring, with 18, 27, and 72 teeth, respectively. The data sets were collected at seven measuring points with gear velocities of 840, 900, 1260, 1470, and 1500 r/min. Vibration signals are acquired at these points. Each speed condition has three gear states: normal, broken, and crack. We selected the gearbox vibration signal at measurement point 3 with a sampling frequency of 51.2 KHz and a speed of 900 rpm. In this section, the length of a single sample is kept the same as in the previous section and 1024 points are chosen as the sample length. This data is used as validation data to evaluate the performance of our proposed methodology. The dataset is partitioned into three unbalanced subsets: A, B, and C, maintaining the identical unbalanced ratio as detailed in the preceding section, as described in Table 3.

The above three unbalanced datasets are tested under 0dB noise conditions to demonstrate the model's effectiveness proposed in this paper. Each experiment is conducted ten times to ensure reliable results, and the average outcome is taken as the final result. The outcomes are presented in Table 4, while the corresponding test result is shown in Fig. 18.

Training was performed under three unbalanced datasets on the laboratory gearbox as shown in Figure 18. An accuracy of about 98% is achieved after the 13th iteration of training with a smooth reduction of losses and no overfitting. This

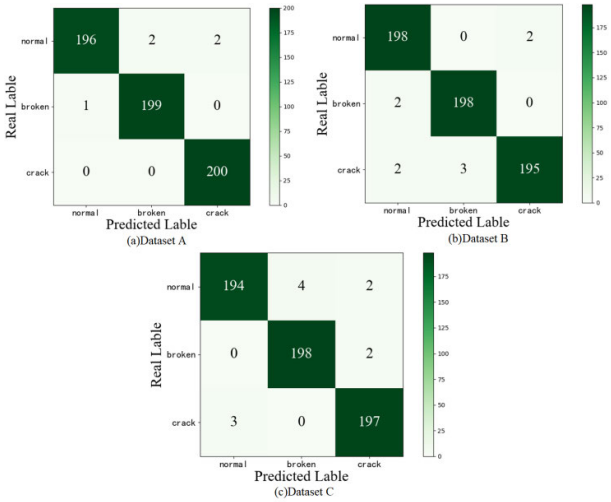

FIGURE 19. Confusion matrix plots on the three datasets in the gearbox experiments.

result emphasizes the robustness and strong convergence ability of the proposed model in this study.

To further observe the performance of the model proposed in this paper on the gearbox dataset, the experimental results are visualized through confusion matrices for the three datasets with varying unbalanced ratios, as shown in Fig. 19.

As shown in Fig. 19, even in the presence of a 0db noise environment, excellent fault identification capability is demonstrated on the three unbalanced datasets, with 99.119%, 98.578%, and 98.128%, respectively, thus further confirming the robustness and generalization capability of the model in this paper.

V. CONCLUSION

The method proposed in this paper is able to solve the problem of low fault classification accuracy due to unbalanced datasets during network model training. Validation is performed on Case Western Reserve University bearing dataset and laboratory planetary gearbox dataset, and the proposed method is compared and analyzed with several other methods to draw the following conclusions:

1) Using a WGAN network with a penalty factor, Such a generative framework can generate realistic data for image augmentation to solve the problem of data imbalance. To obtain the sample input of expanded data, this paper adopts a new conversion method of GADF corresponding to the time series. The obtained image can ensure good temporal correlation and is better than similar methods in the richness of feature information. The effectiveness of the method is verified after theoretical research and experimental comparison.

2) The CBAM-ResNet-GCN network constructed in this paper incorporates the convolutional attention into the residual network, which can effectively extract key information and can obtain a feature matrix. This feature matrix is then used as an input to the graph convolutional neural network, taking advantage of the powerful feature extraction

capabilities of graph convolutional neural networks as well as the ability to utilize edge information. Compared with other models, an accuracy of about 99% was achieved on three unbalanced bearing datasets from Case Western Reserve University, and an accuracy of about 99% was also achieved under four different operating conditions, indicating that the method can efficiently extract fault-related information and improve the fault identification accuracy.

3) This study validates the correlation performance on three unbalanced datasets in an accompanied noise environment. Notably, the fault identification accuracy is close to 98% on the Case Western Reserve University bearing dataset even in the case of -8db strong noise, and to further validate the performance, the fault identification accuracy reaches over 98% on the gearbox dataset containing 0db noise. The robustness and practicality of the model are demonstrated. Consequently, this paper offers a reliable and effective solution for diagnosing rotating machinery faults.

The method proposed in this paper shows excellent performance under the same load, but in the real working environment, it will face the situation of variable load, the method of this paper is not dominant, and migration learning [43] provides a solution to such problems. The next step is to combine the method of this paper with migration learning to solve problems such as data imbalance across working conditions Additionally, there could be interconnections among signals gathered by various sensors. Investigating how to effectively leverage the relationships between multiple sensors to fully exploit valuable information, thereby facilitating easier fault diagnosis, is also a focus of our future research.

ACKNOWLEDGMENT

The authors would like to thank all the peer reviewers for their valuable contributions.

REFERENCES

[1] Y. Xu, Y. Sun, J. Wan, X. Liu, and Z. Song, "Industrial big data for fault diagnosis: Taxonomy, review, and applications," *IEEE Access*, vol. 5, pp. 17368–17380, 2017, doi: 10.1109/ACCESS.2017.2731945.

[2] S. Zhang, S. Zhang, B. Wang, and T. G. Habetler, "Deep learning algorithms for bearing fault diagnostics—A comprehensive review," *IEEE Access*, vol. 8, pp. 29857–29881, 2020, doi: 10.1109/ACCESS.2020.2972859.

[3] Y. Lei, "Deep transfer diagnosis method for machinery in big data era," *J. Mech. Eng.*, vol. 55, no. 7, pp. 1–8, 2019, doi: 10.3901/JME.2019.07.001.

[4] X. Qin, D. Xu, X. Dong, X. Cui, and S. Zhang, "The fault diagnosis of rolling bearing based on improved deep forest," (in english), *Shock Vibrat.*, vol. 2021, pp. 1–13, Jun. 2021, doi: 10.1155/2021/9933137.

[5] Q. Li, Y. Zhou, G. Tang, C. Xin, and T. Zhang, "Early weak fault diagnosis of rolling bearing based on multilayer reconstruction filter," *Shock Vibrat.*, vol. 2021, pp. 1–15, Mar. 2021, doi: 10.1155/2021/6690966.

[6] F. Liu and L. Ren, "Weak fault diagnosis of planetary gearboxes based on maximum correlation kurtosis deconvolution," *Noise Vibrat. Control*, vol. 42, no. 5, pp. 154–158, 2022.

[7] H. Biao, Y. Qin, J. Luo, F. Wu, and D. Xiao, "Rotating machine fault diagnosis by a novel fast sparsity-enabled feature-energy-ratio method," *ISA Trans.*, vol. 136, pp. 417–427, May 2023, doi: 10.1016/j.isatra.2022.10.026.

[8] I. J. Goodfellow, J. Pouget-Abadie, M. Mirza, B. Xu, D. Warde-Farley, S. Ozair, A. Courville, and Y. Bengio, "Generative adversarial networks," 2014, *arXiv.1406.2661*.

[9] J. Yang, J. Liu, J. Xie, C. Wang, and T. Ding, "Conditional GAN and 2-D CNN for bearing fault diagnosis with small samples," *IEEE Trans. Instrum. Meas.*, vol. 70, pp. 1–12, 2021, doi: 10.1109/TIM.2021.3119135.

[10] M. Farajzadeh-Zanjani, E. Hallaji, R. Razavi-Far, and M. Saif, "Generative-adversarial class-imbalance learning for classifying cyber-attacks and faults—A cyber-physical power system," *IEEE Trans. Dependable Secure Comput.*, vol. 19, no. 6, pp. 4068–4081, Nov. 2022, doi: 10.1109/TDSC.2021.3118636.

[11] Y. Li, W. Zou, and L. Jiang, "Fault diagnosis of rotating machinery based on combination of Wasserstein generative adversarial networks and long short term memory fully convolutional network," *Measurement*, vol. 191, Mar. 2022, Art. no. 110826, doi: 10.1016/j.measurement.2022.110826.

[12] H. Gao, X. Zhang, X. Gao, F. Li, and H. Han, "ICoT-GAN: Integrated convolutional transformer GAN for rolling bearings fault diagnosis under limited data condition," *IEEE Trans. Instrum. Meas.*, vol. 72, pp. 1–14, 2023, doi: 10.1109/TIM.2023.3271729.

[13] Z. Du, K. Chen, S. Chen, J. He, X. Zhu, and X. Jin, "Deep learning GAN-based data generation and fault diagnosis in the data center HVAC system," *Energy Buildings*, vol. 289, Jun. 2023, Art. no. 113072, doi: 10.1016/j.enbuild.2023.113072.

[14] T. Han, W. Xie, and Z. Pei, "Semi-supervised adversarial discriminative learning approach for intelligent fault diagnosis of wind turbine," *Inf. Sci.*, vol. 648, Nov. 2023, Art. no. 119496, doi: 10.1016/j.ins.2023.119496.

[15] Q. Qian, J. Zhou, and Y. Qin, "Relationship transfer domain generalization network for rotating machinery fault diagnosis under different working conditions," *IEEE Trans. Ind. Informat.*, vol. 19, no. 9, pp. 9898–9908, Sep. 2023, doi: 10.1109/TII.2022.3232842.

[16] Z. Xing, R. Zhao, Y. Wu, and T. He, "Intelligent fault diagnosis of rolling bearing based on novel CNN model considering data imbalance," *Int. J. Speech Technol.*, vol. 52, no. 14, pp. 16281–16293, Nov. 2022, doi: 10.1007/s10489-022-03196-x.

[17] X. Jiang, J. Zheng, X. Zhuang, and Z. Ge, "Ensemble data augmentation for imbalanced fault diagnosis," *IEEE Trans. Instrum. Meas.*, vol. 72, pp. 1–12, 2023, doi: 10.1109/TIM.2023.3307757.

[18] M. Farajzadeh-Zanjani, E. Hallaji, R. Razavi-Far, M. Saif, and M. Parvania, "Adversarial semi-supervised learning for diagnosing faults and attacks in power grids," *IEEE Trans. Smart Grid*, vol. 12, no. 4, pp. 3468–3478, Jul. 2021, doi: 10.1109/TSG.2021.3061395.

[19] X. Hu, J. Man, H. Yang, J. Deng, and Y. Liu, "An improved metalearning framework to optimize bearing fault diagnosis under data imbalance," *J. Sensors*, vol. 2022, pp. 1–20, Oct. 2022, doi: 10.1155/2022/1809482.

[20] H. Ruan, Y. Wang, X. Li, Y. Qin, and B. Tang, "An enhanced non-local weakly supervised fault diagnosis method for rotating machinery," *Measurement*, vol. 189, Feb. 2022, Art. no. 110433, doi: 10.1016/j.measurement.2021.110433.

[21] S. Zafeiriou, M. Bronstein, T. Cohen, O. Vinyals, L. Song, J. Leskovec, P. Liò, J. Bruna, and M. Gori, "Guest editorial: Non-Euclidean machine learning," *IEEE Trans. Pattern Anal. Mach. Intell.*, vol. 44, no. 2, pp. 723–726, Feb. 2022, doi: 10.1109/TPAMI.2021.3129857.

[22] L. Veyrin-Forrer, A. Kamal, S. Duffner, M. Plantevit, and C. Robardet, "On GNN explainability with activation rules," *Data Mining Knowl. Discovery*, Oct. 2022, doi: 10.1007/s10618-022-00870-z.

[23] G. Huo, Y. Zhang, B. Wang, J. Gao, Y. Hu, and B. Yin, "Hierarchical spatio-temporal graph convolutional networks and transformer network for traffic flow forecasting," *IEEE Trans. Intell. Transp. Syst.*, vol. 24, no. 4, pp. 3855–3867, Apr. 2023, doi: 10.1109/TITS.2023.3234512.

[24] X. Wang, Z. Luo, R. He, and Y. Shao, "Novel medical question and answer system: Graph convolutional neural network based with knowledge graph optimization," *Expert Syst. Appl.*, vol. 227, Oct. 2023, Art. no. 120211, doi: 10.1016/j.eswa.2023.120211.

[25] G. Du, J. Su, L. Zhang, K. Su, X. Wang, S. Teng, and P. X. Liu, "A multi-dimensional graph convolution network for EEG emotion recognition," *IEEE Trans. Instrum. Meas.*, vol. 71, pp. 1–11, 2022, doi: 10.1109/TIM.2022.3204314.

[26] M. Zhang, Z. Zhen, N. Liu, H. Zhao, Y. Sun, C. Feng, and F. Wang, "Optimal graph structure based short-term solar PV power forecasting method considering surrounding spatio-temporal correlations," *IEEE Trans. Ind. Appl.*, vol. 59, no. 1, pp. 345–357, Jan. 2023, doi: 10.1109/TIA.2022.3213008.

[27] T. Li, Z. Zhou, S. Li, C. Sun, R. Yan, and X. Chen, "The emerging graph neural networks for intelligent fault diagnostics and prognostics: A guideline and a benchmark study," *Mech. Syst. Signal Process.*, vol. 168, Apr. 2022, Art. no. 108653, doi: 10.1016/j.ymssp.2021.108653.

[28] C. Li, L. Mo, and R. Yan, "Fault diagnosis of rolling bearing based on WHVG and GCN," *IEEE Trans. Instrum. Meas.*, vol. 70, pp. 1–11, 2021, doi: 10.1109/TIM.2021.3087834.
[29] B. Zhang, X. Pang, P. Zhao, and K. Lu, "A new method based on encoding data probability density and convolutional neural network for rotating machinery fault diagnosis," *IEEE Access*, vol. 11, pp. 26099–26113, 2023, doi: 10.1109/ACCESS.2023.3257041.
[30] M. Arjovsky, S. Chintala, and L. Bottou, "Wasserstein GAN," 2017, *arXiv.1701.07875*.
[31] I. Gulrajani, F. Ahmed, M. Arjovsky, V. Dumoulin, and A. Courville, "Improved training of Wasserstein GANs," 2017, *arXiv:1704.00028*.
[32] S. Ning, Y. Ren, and Y. Wu, "Intelligent fault diagnosis of rolling bearings based on the visibility algorithm and graph neural networks," *J. Brazilian Soc. Mech. Sci. Eng.*, vol. 45, no. 2, Feb. 2023, doi: 10.1007/s40430-022-03913-0.
[33] L. Wang, Y. Cao, S. Wang, X. Song, S. Zhang, J. Zhang, and J. Niu, "Investigation into recognition algorithm of helmet violation based on YOLOv5-CBAM-DCN," *IEEE Access*, vol. 10, pp. 60622–60632, 2022, doi: 10.1109/ACCESS.2022.3180796.
[34] T. Li, Z. Zhao, C. Sun, R. Yan, and X. Chen, "Domain adversarial graph convolutional network for fault diagnosis under variable working conditions," *IEEE Trans. Instrum. Meas.*, vol. 70, pp. 1–10, 2021, doi: 10.1109/TIM.2021.3075016.
[35] W. Gao, H. Jin, and G. Yang, "Series arc fault diagnosis method of photovoltaic arrays based on GASF and improved DCGAN," *Adv. Eng. Informat.*, vol. 54, Oct. 2022, Art. no. 101809, doi: 10.1016/j.aei.2022.101809.
[36] W. Zhang, T. Lin, H. Wang, and L. Song, "ConvNeXt-CNN based intelligent fault diagnosis method for rotating equipment," in *Proc. Int. Conf. Sens., Meas. Data Anal. Era Artif. Intell. (ICSMD)*, Harbin, China, Nov. 2022, pp. 1–6, doi: 10.1109/ICSMD57530.2022.10058420.
[37] J. Guo, M. Wang, L. Sun, and D. Xu, "A new approach to fault diagnosis of rolling bearing unbalance dataset based on raw generative adversarial networks," *Comput. Integr. Manuf. Syst.*, vol. 28, no. 8, pp. 2825–2835, 2022, doi: 10.13196/j.cims.2022.09.015.
[38] C.-Y. Lee and W.-C. Lin, "Induction motor fault classification based on ROC curve and t-SNE," *IEEE Access*, vol. 9, pp. 56330–56343, 2021, doi: 10.1109/ACCESS.2021.3072646.
[39] Y. Sun, S. Liu, T. Zhao, Z. Zou, B. Shen, Y. Yu, S. Zhang, and H. Zhang, "A new hydrogen sensor fault diagnosis method based on transfer learning with LeNet-5," *Frontiers Neurorobotics*, vol. 15, May 2021, doi: 10.3389/fnbot.2021.664135.
[40] K. He, X. Zhang, S. Ren, and J. Sun, "Deep residual learning for image recognition," 2015, *arXiv:1512.03385*.
[41] D. Zhang, E. Stewart, M. Entezami, C. Roberts, and D. Yu, "Intelligent acoustic-based fault diagnosis of roller bearings using a deep graph convolutional network," *Measurement*, vol. 156, May 2020, Art. no. 107585, doi: 10.1016/j.measurement.2020.107585.
[42] X. Yu, B. Tang, J. Wei, and L. Deng, "Fault diagnosis for aero-engine accessory gearbox by adaptive graph convolutional networks under intense background noise conditions," *Chinese J. Sci. Instrum.*, vol. 42, no. 8, pp. 78–86, 2021, doi: 10.19650/j.cnki.cjsi.J2107732.
[43] J. Yao and T. Han, "Data-driven lithium-ion batteries capacity estimation based on deep transfer learning using partial segment of charging/discharging data," *Energy*, vol. 271, May 2023, Art. no. 127033, doi: 10.1016/j.energy.2023.127033.

HAITAO WANG received the master's degree in electrical theory and new technology and the Ph.D. degree in electronic science and technology from Northwestern Polytechnical University, China, in 2009 and 2013, respectively. He is currently a Professor with Xi'an University of Architecture and Technology, China, where he is also the Director of the Electromechanical System Detection and Control Research Institute. His current research interests include deep learning, fault diagnosis and prediction, and reliability analysis.

XIYANG DAI received the bachelor's degree in mechanical engineering from Shaanxi University of Technology, in 2022. He is currently pursuing the master's degree in mechanical and electrical engineering with Xi'an University of Architecture and Technology. His current research interests include information fusion, the fault diagnosis of rotating machinery, and intelligent equipment operation and maintenance based on big data driving.

LICHEN SHI received the master's degree in mechanical engineering and the Ph.D. degree in electronic science and technology from Xi'an University of Architecture and Technology, China, in 1998 and 2009, respectively. She is currently a Professor with Xi'an University of Architecture and Technology and the Executive Director of Shaanxi Vibration Engineering Society. Her current research interests include deep learning, mechanical system dynamics, equipment condition monitoring, and fault diagnosis.

MINGJUN LI received the bachelor's degree in mechanical engineering from Xi'an University of Architecture and Technology, in 2022, where he is currently pursuing the master's degree in mechanical and electrical engineering. His current research interests include information fusion, the fault diagnosis of rotating machinery, intelligent equipment operation, and flexible sensor preparation.

ZELIN LIU received the bachelor's degree in mechanical engineering from Xi'an University of Architecture and Technology, in 2022, where he is currently pursuing the master's degree in mechanical and electrical engineering. His current research interests include information fusion, the fault diagnosis of rotating machinery, intelligent equipment operation, and nonlinear system identification.

RUIHUA WANG received the bachelor's degree in mechanical engineering from Xi'an University of Aeronautics, in 2021. She is currently pursuing the master's degree in mechanical and electrical engineering with Xi'an University of Architecture and Technology. Her current research interests include fault diagnosis and life prediction of electromechanical equipment.

XIAOHUA XIA received the bachelor's degree in mechanical engineering from China University of Petroleum, in 2009, and the Ph.D. degree in mechanical engineering from Xi'an Jiaotong University, in 2015. He is currently an Associate Professor and a Doctoral Supervisor with Chang'an University. His main research interests include machine vision and opto-mechatronics.